FERMILAB-PUB-15-688-APC
ACCEPTED
February 2015

VALIDATION OF MONTE CARLO SIMULATION OF NEUTRON PRODUCTION IN A SPALLATION EXPERIMENT[1,2]

L. Zavorka [a,b,3], J. Adam [a,c], M. Artiushenko [d], A.A. Baldin [a], V.B. Brudanin [a], O. Bukhal [e], P. Caloun [c], V.V. Chilap [f], W.I. Furman [a], K. Husak [e], M.G. Kadykov [a,+], K. Katovsky [g], J. Khushvaktov [a], I.I. Marin [a], V.S. Pronskikh [a,h], A.A. Solnyshkin [a], V. Sotnikov [d], V.I. Stegailov [a], M. Suchopar [b,c], O. Svoboda [c], V.M. Tsoupko-Sitnikov [a], S.I. Tyutyunnikov [a], V. Voronko [d], J. Vrzalova [a,b,c], V. Wagner [c], P. Zhivkov [i], I. Zhuk [e]

[a] *Joint Institute for Nuclear Research, Dubna 141980, Russia*
[b] *Faculty of Nuclear Sciences and Physical Engineering, Czech Technical University, Prague 11519, Czech Republic*
[c] *Nuclear Physics Institute of the ASCR, Řež 25068, Czech Republic*
[d] *National Science Center Kharkov Institute of Physics and Technology, Kharkov 61108, Ukraine*
[e] *Joint Institute of Power and Nuclear Research NASB, Sosny, Minsk 220109, Belarus*
[f] *Center of Physics and Technical Projects "Atomenergomash", Moscow 125130, Russia*
[g] *Brno University of Technology, Brno 60200, Czech Republic*
[h] *Fermi National Accelerator Laboratory, Batavia IL 60510-5011, USA*
[i] *Institute for Nuclear Research and Nuclear Energy, Bulgarian Academy of Sciences, Sofia 1784, Bulgaria*

A renewed interest in experimental research on Accelerator-Driven Systems (ADS) has been initiated by the global attempt to produce energy from thorium as a safe(r), clean(er) and (more) proliferation-resistant alternative to the uranium-fuelled thermal nuclear reactors. The ADS research has been actively pursued at the Joint Institute for Nuclear Research (JINR), Dubna, since decades. Most recently, the emission of fast neutrons was experimentally investigated at the massive (m = 512 kg) natural uranium spallation target *QUINTA*. The target has been irradiated with the relativistic deuteron beams of energy from 0.5 AGeV up to 4 AGeV at the JINR Nuclotron accelerator in numerous experiments since 2011. Neutron production inside the target was studied through the gamma-ray spectrometry measurement of natural uranium activation detectors. Experimental reaction rates for (n, γ), (n,f) and (n,2n) reactions in uranium has provided valuable information about the neutron distribution over a wide range of energies up to some GeV. The experimental data were compared to the predictions of Monte Carlo simulations using the MCNPX 2.7.0 code. The results are presented and potential sources of partial disagreement are discussed later in this work.

---

[1] Fermilab is operated by Fermi Research Alliance, LLC under Contract No. De-AC02-07CH11359 with the US Department of Energy.
[2] Accepted to Annals of Nuclear Energy
[3] zavorka@lanl.gov

Validation of Monte Carlo Simulation of Neutron Production in a Spallation Experiment

L. Zavorka [a,b,*], J. Adam [a,c], M. Artiushenko [d], A.A. Baldin [a], V.B. Brudanin [a], O. Bukhal [e], P. Caloun [c], V.V. Chilap [f], W.I. Furman [a], K. Husak [e], M.G. Kadykov [a,+], K. Katovsky [g], J. Khushvaktov [a], I.I. Marin [a], V.S. Pronskikh [a,h], A.A. Solnyshkin [a], V. Sotnikov [d], V.I. Stegailov [a], M. Suchopar [b,c], O. Svoboda [c], V.M. Tsoupko-Sitnikov [a], S.I. Tyutyunnikov [a], V. Voronko [d], J. Vrzalova [a,b,c], V. Wagner [c], P. Zhivkov [i], I. Zhuk [e]

[a] *Joint Institute for Nuclear Research, Dubna 141980, Russia*
[b] *Faculty of Nuclear Sciences and Physical Engineering, Czech Technical University, Prague 11519, Czech Republic*
[c] *Nuclear Physics Institute of the ASCR, Řež 25068, Czech Republic*
[d] *National Science Center Kharkov Institute of Physics and Technology, Kharkov 61108, Ukraine*
[e] *Joint Institute of Power and Nuclear Research NASB, Sosny, Minsk 220109, Belarus*
[f] *Center of Physics and Technical Projects "Atomenergomash", Moscow 125130, Russia*
[g] *Brno University of Technology, Brno 60200, Czech Republic*
[h] *Fermi National Accelerator Laboratory, Batavia IL 60510-5011, USA*
[i] *Institute for Nuclear Research and Nuclear Energy, Bulgarian Academy of Sciences, Sofia 1784, Bulgaria*

* Corresponding author.
E-mail address: zavorka@jinr.ru (L. Zavorka)

[+] Deceased.

Highlights:

- Uranium spallation target was irradiated by up to 4 AGeV deuteron beams.
- Neutron production was investigated through (n,γ), (n,f), and (n,2n) reactions in ^{nat}U.
- Reaction rates were also calculated employing the MCNPX 2.7.0 code.
- Agreement between experiment and simulation of neutron-induced reactions was found.
- Overestimation in simulation of production of charged particles is discussed.

Keywords:
Accelerator-driven systems
Uranium spallation target
Neutron emission
Activation measurement
Monte Carlo simulation

Abstract

A renewed interest in experimental research on Accelerator-Driven Systems (ADS) has been initiated by the global attempt to produce energy from thorium as a safe(r), clean(er) and (more) proliferation-resistant alternative to the uranium-fuelled thermal nuclear reactors. The ADS research has been actively pursued at the Joint Institute for Nuclear Research (JINR), Dubna, since decades. Most recently, the emission of fast neutrons was experimentally investigated at the massive (m = 512 kg)

natural uranium spallation target *QUINTA*. The target has been irradiated with the relativistic deuteron beams of energy from 0.5 AGeV up to 4 AGeV at the JINR Nuclotron accelerator in numerous experiments since 2011. Neutron production inside the target was studied through the gamma-ray spectrometry measurement of natural uranium activation detectors. Experimental reaction rates for (n,γ), (n,f) and (n,2n) reactions in uranium has provided valuable information about the neutron distribution over a wide range of energies up to some GeV. The experimental data were compared to the predictions of Monte Carlo simulations using the MCNPX 2.7.0 code. The results are presented and potential sources of partial disagreement are discussed later in this work.

1. Introduction

1.1. Research on Accelerator-Driven Systems

A challenging worldwide research on a subcritical electro-nuclear production of neutrons for both energy generation from thorium and nuclear waste transmutation was vigorously launched in the 1990s when C. Rubbia and C. Bowman introduced their enthusiastic projects for utilization of fast- and thermal-neutron spectrum in Accelerator-Driven Systems [1],[2]. Since then, the experimental investigation of neutron production in thick heavy-metal spallation targets has become of great importance in many scientific laboratories all over the globe [3]-[7].

At present, after a short period of decline in ADS research over the last few years, thorium appears to be reconsidered as a promising candidate for feeding the future subcritical nuclear systems in the form of fuel dissolved in a liquid salt, such as in the Accelerator Molten Salt Breeder (AMSB) [8],[9]. Thorium is also expected to be used in the Relativistic Nuclear Technology (RNT) [10] - another auspicious design based on ADS principles.

The main features of RNT are i) a deep subcritical core made of thorium or natural uranium and ii) energy of beams of accelerated particles (protons, deuterons) impinging on the spallation target increased up to approx. 10 GeV. In such facilities with a minimal neutron leakage, a maximally hard neutron spectrum will serve for nuclear energy production and effective transmutation of spent nuclear fuel and long-lived radioactive waste.

The advantages of the substantially increased beam energy should be as follows. In the 1990s, Yurevich et al. [11],[12] performed a series of experiments with a thick lead spallation target irradiated with proton and deuteron beams of various energies up to 4 GeV. According to the results, the higher the kinetic energy of beam particles, the harder the spectrum of neutrons generated inside the spallation target. One can benefit from this increase through the additional neutron production via inelastic (n,*x*n) reactions. Moreover, as shown in [13] and other related studies [14]-[16], with the increasing energy of neutrons also grow both the mean kinetic energy and multiplicity of neutrons produced in fission of some actinides induced by high-energy neutrons. Nevertheless, the above mentioned phenomena need to be experimentally studied in more detail at a large-scale quasi-infinite spallation targets with a minimal neutron leakage.

Following numerous experiments with the lead-paraffin [17], lead-graphite [18], and lead-uranium [19] spallation target-blanket assemblies, a current research interest of the international collaboration "Energy and Transmutation of Radioactive Waste" [20], based at JINR, is focused on the experimental research on neutron production at the massive natural uranium spallation target *QUINTA* that represents a central region of the quasi-infinite uranium spallation target. The experiments also serve as a tool for validation of Monte Carlo radiation transport programs and available physics models.

1.2. Main purposes of the experiment

Cross sections for the radiative capture (n,γ), inelastic reactions (n,*x*n), and fission (n,f) in natural uranium cover a wide range of neutron energies (see **Fig. 1a**). These reactions provide valuable

information on the neutron spectrum inside the uranium spallation target. With respect to that, a series of experiments was carried out with the following aims:

i) to determine the experimental reaction rates for (n,γ), (n,2n), and (n,f) reactions in natural uranium samples situated inside the *QUINTA* target in a position where the maximum neutron flux is expected in order to reach sufficient statistics of the conducted gamma-ray spectrometry measurements. To fulfill this requirement, the irradiation position of the samples was selected by taking into consideration the results of previous experiments with the deuteron beams and the lead-uranium spallation target «Energy plus Transmutation» [21];
ii) to perform simulations of neutron, proton, and deuteron spectra inside the *QUINTA* target using a careful replica of the target and the INCL-ABLA physics models available in the MCNPX 2.7.0 code;
iii) finally, to compare the experimental reaction rates to the results of simulation and try to find out a potential source of disagreement, if any occurred.

2. Experimental arrangement

2.1. Target setup

The *QUINTA* target [22] is a thick spallation target composed of 512 kg of natural uranium. The whole uranium target, as schematically illustrated in **Fig. 2**, consists of five hexagonal prism-shaped sections (height 350 mm, length 114 mm) with a 17 mm air gap between each other. All sections are filled with uranium cylinders. The front section with a central uranium-free hole, which serves as a beam window, contains 54 uranium cylinders. The other sections are composed of 61 uranium cylinders. The cylinders are 104 mm long and 36 mm in diameter. A length of the whole target is 638 mm.
With respect to safety requirements, each uranium cylinder is encapsulated in a 1 mm thick aluminium casing. The cylinders of every target section are inserted into a casing made of a 5 mm thick aluminium sheet. The aluminium plates 2 mm in thickness serve as a holder for the investigated uranium samples and are located in the air gaps between the target sections.
Natural uranium is certainly main but not the only construction material of the target. Moreover, since 2012, the whole target has been surrounded by a shielding that is constructed of lead bricks with a thickness of 100 mm and serves as a supplementary neutron reflector. A square hole of 150×150 mm^2 in the front side of the shielding serves as a beam window. The angle between the target axis and deuteron beam is 2°. Such geometry should avoid passing the beam through the target without any interaction.

2.2. Natural uranium samples

The investigated samples made of natural uranium are cylinders 14 mm in diameter. The minimum mass and thickness of the sample were 0.15 g and 50 μm, respectively. The sample with a maximum mass of 0.50 g was 200 μm thick. Different thickness was taken into consideration when calculating a correction factor for self-attenuation of gamma rays in the samples.
Some uranium samples were covered by a 1 mm thick cadmium layer in order to exclude a potential contribution of thermal neutrons – moderated inside the target and scattered from the surroundings – to the fission of ^{235}U in natural uranium.
As shown in **Fig. 2,** the uranium samples were located on the aluminium holder between the second and the third section of the target directly on the longitudinal axis. In this position, the maximum neutron flux was expected and later confirmed in the experimental study [23].

2.3. Beam characteristics

A series of experiments was carried out in the years 2011-2012. The deuteron beams of kinetic energy per nucleon E_d = 0.5, 1, 2, 3, and 4 AGeV and the total number of deuterons in the order of $10^{12} \div 10^{13}$ were provided by the JINR Nuclotron accelerator.

The integral number of deuterons N_d colliding with the target was determined with the use of aluminium activation monitors with at least two completely independent set of data (different position and thickness of monitors, measurement with different HPGe detectors, independent data analysis). The beam monitors were situated at a distance between 94 cm and 300 cm from the target in order to minimize the impact of the back-scattered neutrons by means of the ^{27}Al(n,α)^{24}Na reaction with the energy threshold approx. 3 MeV. A reaction rate of the ^{27}Al(d,3p2n)^{24}Na reaction was measured to calculate the beam integral. The experimental data were corrected for fluctuation of beam intensity during the irradiation using the information from the gas-filled fast ionization chambers. For further details on beam monitoring and corresponding cross-section values see [24]. The basic characteristics of deuteron beams are listed in **Table 1**.

Despite every effort, the deuteron beam did not hit exactly the centre of the front side of the target. For this reason, the coordinates of the centre of the beam and FWHM of a Gaussian profile of the beam in the beam window (on the X- and Y-axis, perpendicular to the beam axis) were measured with the solid state nuclear track detectors (SSNTD). The measurement technique [25] is based on correlation between the track density and flux of the incident deuteron beam. The SSNTDs were composed of natural lead irradiator and artificial mica (Fluorophlogopite). In addition, the beam profile was monitored with copper activation monitors. The results were used to calculate the radial distance R_{beam} between the uranium samples and centre of the beam.

Table 1 Parameters of the deuteron beams and positions of the samples during the experiments carried out in 2011-2012. Statistical and systematic uncertainties are indicated for the beam integral determination. Systematic uncertainty 10% comes from determination of the ^{27}Al(d,3p2n)^{24}Na cross section. The sign "Cd" means that the uranium sample was covered by a 1 mm thick cadmium layer.

Experiment Identification	**Beam Energy** E_d (AGeV)	**Beam Integral** $N_d \times 10^{13}$ (deuterons)	**FWHM$_X$; FWHM$_Y$** (mm)	**Sample-to-beam axis distance** R_{beam} (mm)
March 2011 (M11)	**1**	1.44 ± 0.14 ± 0.14	20; 28	12 ± 2
	2	1.42 ± 0.18 ± 0.14	22; 23	13 ± 2
	3	1.94 ± 0.20 ± 0.19	39; 31	19 ± 2
March 2012 (M12, M12-Cd)	**0.5**	1.86 ± 0.05 ± 0.19	29; 32	14 ± 2, $^{Cd:}$11 ± 2
	2	2.72 ± 0.07 ± 0.27	11; 12	9 ± 2, $^{Cd:}$22 ± 2
	4	0.37 ± 0.08 ± 0.04*	9; 12	5 ± 2, $^{Cd:}$12 ± 2

* The data of NPI Rez and JINR Dubna could have been influenced by the secondary neutrons during this run. For this reason, the data of NSC Kharkov considered only.

2.4. Experimental data acquisition and analysis

After irradiation, the uranium samples were transported to the gamma-ray spectrometry laboratory. Measurements were carried out using the n-type coaxial HPGe detector CANBERRA GR1819 of the relative efficiency 18% and resolution FWHM = 1.8 keV at 1.33 MeV. The spectrometer operates in a shielding made of thick lead blocks including additional copper and cadmium plates inside. The spectroscopy amplifier CANBERRA 2024 and multichannel analyzer ORTEC 927 ASPEC were used for further processing of the electronic signal from the detector's preamplifier.

The semiconductor detector is well calibrated in the energy region from 60 keV up to approx. 3 MeV. Measurements of the full-energy-peak efficiency at a position of 18 mm from the beryllium window were performed using the following standard gamma-ray sources: ^{22}Na, ^{44}Ti, ^{54}Mn, ^{57}Co, ^{60}Co, ^{65}Zn, ^{88}Y, ^{109}Cd, ^{113}Sn, ^{133}Ba, ^{137}Cs, ^{139}Ce, ^{152}Eu, ^{207}Bi, ^{228}Th, and ^{241}Am. Because of the close source-

detector geometry, a correction for gamma coincidence summing was performed. Moreover, the experimental efficiency was compared to the results of the Monte Carlo simulation of the detector efficiency using a detailed scheme of the detector provided by the manufacturer. The efficiency calibration was corrected for the area-source geometry (natural uranium samples) using the results of simulation.
Measurements of the uranium samples started usually one hour after the end of irradiation. A period of data acquisition was gradually increased from 10 min up to 6 days. The samples were measured at least ten times in order to reach the results for both relatively short- and long-lived reaction products. The gamma-ray spectra were processed using the DEIMOS32 code [26]. A count area of the full-energy peaks was fitted by the Gaussian function. The identification of the processed peaks was based on the gamma-ray energy, intensity, and half-life of produced nuclei.
A total production of a residual nucleus in a sample can be determined by the calculation of the reaction rate. It is defined as a number of produced nuclei of a radionuclide per one atom of the uranium sample N_a and one deuteron colliding with the spallation target per one second N_d. The experimental reaction rate R_{exp} is calculated according to the formula:

$$R_{exp} = \frac{S\lambda \frac{t_{real}}{t_{live}}}{N_a N_d \varepsilon_{eff} I_\gamma (1 - e^{-\lambda t_{irr}}) e^{-\lambda t_{cool}} (1 - e^{-\lambda t_{real}}) \eta_\alpha \eta_\beta \eta_\gamma \eta_\delta} \quad (1)$$

where S is the area of the full-energy peak of the gamma line of intensity I_γ, λ is the decay constant, t_{real} is the time of measurement, t_{live} the time of measurement corrected for dead time, t_{cool} the cooling time, t_{irr} represents the time of irradiation, and ε_{eff} is the full-energy-peak efficiency. The symbols η_α, η_β, η_γ, and η_δ are the correction coefficients for the area-source efficiency, beam instability, self-attenuation of gamma rays in the sample, and for true coincidence summing. A measurement unit of the reaction rate is (atom^{-1}·deuteron^{-1}). Gamma-ray energies and intensities for the isotope identification as well as half-lives and internal-conversion coefficients α for performing coincidence summing corrections were taken from the ENSDF database [27] and WWW Table of Radioactive Isotopes [28].
The experimental variance was determined as a maximum of the internal and external variance, as recommended in [29]. A total uncertainty of the experimental data was calculated according to the error propagation law of Gauss taking into consideration the uncertainty in determination of the cross section for the beam monitoring (10%), determination of the detector efficiency (3%), determination of the mass of samples (0.1%), uncertainty in nuclear data provided by literature and statistical uncertainty in the peak area analysis (generally not exceeding 5%).

3. Calculation of particle production

The Monte Carlo simulation of particle spectra in the position of the natural uranium samples inside the *QUINTA* target allows us to calculate the reaction rate and make a comparison with the experimental results. The calculated reaction rate R_{calc} is determined according to the following equation

$$R_{calc} = \sum_{k=1}^{3} \sum_{i=1}^{n} R_i^k = \sum_{k=1}^{3} \sum_{i=1}^{n} \phi_i^k \sigma_i^k \Delta E_i \quad (2)$$

where ϕ_i^k is the flux of particles k (neutrons, deuterons, protons) in cm^{-2} per one beam particle and width ΔE_i of the energy bin i, in which the reaction cross section has a value of σ_i^k. The total reaction rate is defined as a sum of partial reaction rates R_i^k.
The ratio $E/C = R_{exp}/R_{calc}$ serves as a comparison between the experimental and calculated reaction rates.

3.1. Monte Carlo simulation

A careful replica of the *QUINTA* target was prepared [30]. The MCNPX 2.7.0 code [31] was used for calculation of neutron, proton, and deuteron flux. To calculate the flux, the cross-section data library ENDF/B-VII.0 [32], intranuclear physics model INCL4 [33], and the ABLA fission-evaporation event generator [34] were selected with respect to the previous experiences with the Monte Carlo simulation of neutron distribution in the spallation targets [18],[30]. The experimental characteristics of the Gaussian profile of the deuteron beam were included into the MCNPX simulations.
An example of simulation of neutron spectrum inside the natural uranium sample during the irradiation with the 2 AGeV deuteron beam is shown in **Fig. 1b**. A convolution of the neutron flux and the cross-section for the (n,γ), (n,2n), and (n,f) reactions, i.e. the calculated reaction rate for the (n,γ) and (n,2n) reactions in ^{238}U and the (n,f) reaction in ^{nat}U, are presented in **Fig. 1c**. A comparison of neutron, proton, and deuteron spectra in the uranium sample is presented in **Fig. 3**.
According to [19], the influence of gamma- and pion-induced fission of natural uranium in a similar spallation experiment does not exceed 1.8% of the total number of fission events and was not taken into consideration in this work. Total statistical uncertainty of the MCNPX simulation was below 1%.

3.2. Cross section determination

In order to calculate the reaction rate according to Eq. (2), the cross sections for (n,γ), (n,f) and (n,2n) reactions in uranium were taken from the nuclear data library ENDF/B-VII.0 up to energy 20 MeV. Above this value, the JENDL-HE/2007 [35] data file was used for (n,γ) and (n,f). This library provides cross sections up to the neutron energy 3 GeV. At higher energies, the data were extrapolated. The TALYS-1.6 [36],[37] nuclear reaction program was employed to calculate the cross section for the (n,2n) reaction in ^{238}U from 20 MeV up to 1 GeV. TALYS was also used for calculation of proton- and deuteron-induced production of ^{237}U and ^{239}Np, a daughter of ^{239}U. Excluding the data from TALYS, the cross sections were processed into the structure of energy bins of the simulation of neutron spectra using the NJOY 99.393 [38] code system.
As regards the charged-particle-induced fission cross section, since no data are provided in the ENDF/B-VII.0 library for uranium, the JENDL-HE/2007 file was used for determination of the proton-induced fission cross section. Unfortunately, even this data file does not contain any data on deuteron-induced fission. The deuteron-induced fission cross section for ^{238}U was determined as follows: as can be seen in **Fig. 4**, the JENDL-HE/2007 evaluated data on (p,f) reaction are not in contradiction to the numerous experimental data available in the EXFOR database [39]-[48] – contrary to the TENDL-2013 [49] library, which also provides the (p,f) cross sections up to 200 MeV. On the other hand, there are very few experimental data on the (d,f) reaction in ^{238}U above 100 MeV [42],[48]. The (d,f) cross section was determined on the basis of the average ratio of the experimental (d,f) data to the JENDL-HE/2007 evaluated (p,f) data, which equals 1.48 above 100 MeV. Thus the JENDL-HE/2007 (p,f) data multiplied by this value are considered to be the best option for the (d,f) cross section in this work. Here again, above the energy 3 GeV, the cross sections were extrapolated.

4. Results of measurements

In most cases, both the ^{237}U and ^{239}U nuclei are produced from ^{238}U through the interactions with spallation and fission neutrons. At GeV energies, the cross section for proton- and deuteron-induced production of these isotopes is insignificant in comparison with the (n,2n) and (n,γ) cross sections across the whole energy spectrum of neutrons generated in the spallation target.

The ^{238}U(n,2n)^{237}U reaction rate can be measured directly through the production of ^{237}U (half-life $T_{1/2}$ = 6.8 d). A direct product of the ^{238}U(n,γ)^{239}U reaction has a relatively short half-life 23.5 min. For this reason, the production of ^{239}U was measured through its daughter in β^-decay – ^{239}Np ($T_{1/2}$ = 2.4 d) after ten half-lives of ^{239}U have elapsed. The ^{239}Np isotope then decays into ^{239}Pu. The experimental reaction rates of the ^{238}U(n,2n)^{237}U and ^{238}U(n,γ)^{239}U reactions in the natural uranium samples are presented in **Table 2** and **Table 3**, respectively.

Fission of uranium in the central region of the *QUINTA* target can be initiated by spallation neutrons, fission neutrons, neutrons released in the (n,*x*n) reactions, and neutrons scattered from the surrounding materials. In addition, fission can also be provoked not only by primary deuterons, but also by protons released in the deuteron break-up or in the intranuclear cascade. Since both the energy spectrum and quantity of the charged particles are limited in comparison with a wide spectrum of produced neutrons (see **Fig. 3**), their contribution to the total fission rate will be less important, but not insignificant in comparison with neutrons.

Taking this into consideration, the mean value of the reaction rate for fission was determined on the basis of the experimental reaction rates of the identified fission products and the neutron fission yield data. A wide series of the produced fission fragments was selected: ^{85m}Kr, ^{87}Kr, ^{88}Kr, ^{91}Sr, ^{92}Sr, ^{93}Y, ^{95}Zr, ^{97}Zr, ^{99}Mo, ^{103}Ru, ^{105}Ru, ^{107}Rh, ^{113}Ag, ^{115}Cd, ^{117m}Cd, ^{117}Cd, ^{125}Sn, ^{127}Sb, ^{129}Sb, ^{131}I, ^{133}I, ^{134}Te, ^{135}I, ^{140}Ba, ^{143}Ce, ^{147}Nd, and ^{149}Nd. These fission products have the gamma-ray energies as well as intensities suitable for measurements with the HPGe detectors. Moreover, these fragments were selected with respect to their half-life, which is much longer than the half-life of the parent nucleus and all the predecessors in the β^-decay chain, so that one can use the cumulative fission yields. The cumulative yields were taken from the ENDF/B-VII.1 data library [50].

The ENDF/B-VII.1 library provides the fission yields for ^{235}U at energy of neutrons 25.3 meV, 500 keV, and 14 MeV. Fission yields for 500-keV and 14-MeV neutrons are available for ^{238}U. Obviously, the fission yields for natural uranium should consist of fission yields for both ^{235}U and ^{238}U.

In the "first estimation" (F.E.) method – without any knowledge of the results of simulation of neutron spectra – it was considered that i) the main contribution to the fission of ^{238}U have the high energy neutrons and ii) there are some scattered thermal and low-energy neutrons that can initiate fission of ^{235}U with the cross section considerably higher in comparison with fast neutrons. For this reason, the fission yield Y_z^{nat} for the fission fragment z produced in natural uranium was calculated according to the following equation:

$$Y_z^{nat} = a^{235} Y_z^{235}(E_n^{25.3\ meV}) + a^{238} Y_z^{238}(E_n^{14\ MeV}) \quad (3)$$

where a^{235} = 0.72% and a^{238} = 99.28% are the abundances of ^{235}U and ^{238}U, respectively, in natural uranium, Y_z^{235} is the fission yield of the fission product z released in the fission of ^{235}U induced by neutrons of energy 25.3 meV. Similarly, Y_z^{238} is the fission yield of the same fission fragment produced in ^{238}U by neutrons of energy 14 MeV.

The calculation of the fission yields in the "spectrum considered" (S.C.) method is based on the results of the Monte Carlo simulation of neutron spectra. The whole interval of the neutron energies from thermal energies up to GeV energies can be divided into three regions: i) thermal and low-energy with a maximum neutron energy E_n = 251 keV, ii) unresolved resonance and fast, in which 251 keV ≤ E_n < 6.31 MeV, and iii) high-energy where the minimum energy of neutrons starts at 6.31 MeV. The boundaries correspond approximately to the mean energy between 25.3 meV and 500 keV and between

500 keV and 14 MeV, taking into account the structure of energy bins of the simulated neutron flux. The calculated fission reaction rate in a given energy region m related to the total fission rate gives the weighting factor w_m, where $\sum w_m = 1$. The weighted fission yields $Y_{z,w}^{nat}$ in natural uranium are determined as follows:

$$Y_{z,w}^{235} = \sum_{m=1}^{3} w_m \, Y_{z,w}^{235}(E_n^m) \tag{4}$$

$$Y_{z,w}^{238} = \sum_{m=1}^{2} w_m \, Y_{z,w}^{238}(E_n^m) \tag{5}$$

$$Y_{z,w}^{nat} = a^{235} Y_{z,w}^{235} + a^{238} Y_{z,w}^{238} \tag{6}$$

Here, $Y_{z,w}^{235}(E_n^m)$ are the cumulative fission yields in ^{235}U at energies 25.3 meV, 500 keV, and 14 MeV, $Y_{z,w}^{238}(E_n^m)$ are the yields in ^{238}U at energies 500 keV and 14 MeV. The $Y_{z,w}^{235}$ and $Y_{z,w}^{238}$ are the cumulative fission yields for ^{235}U and ^{238}U, respectively. Regarding ^{238}U, the number of intervals is reduced due to the lack of the fission yield data for thermal neutrons. Consequently, the only boundary is E_n= 6.31 MeV in this case.
Finally, the experimental reaction rate for fission is calculated as a weighted mean of the reaction rates of the identified fission products divided by the corresponding fission yields. The experimental results on fission rates – employing both the F.E. and S.C. methods – are presented in **Table 5**. One can clearly see that there is a good agreement between one another. This means that the fission rate can be reliably determined without performing simulations of neutron flux. The ratios of the experimental reaction rate to the cumulative fission yield for the selected fission fragments are presented in **Table 7** in Appendix to this article.

5. Comparison of the experimental data and simulation

In the following subsections, a comparison of the experimental reaction rates to the calculated production of ^{237}U and ^{239}U as well as fission rate in the natural uranium samples is discussed.

5.1. Production of ^{237}U

The determination of production of ^{237}U from ^{238}U according to Eq. (2) – using the MCNPX 2.7.0 code to calculate the particle flux and ENDF/B-VII.0 ($E_n \leq 20$ MeV), JENDL-HE/2007 ($E_n > 20$ MeV), and TALYS (proton-, deuteron-induced reactions) for calculation of the cross sections – has shown that the ^{237}U isotope is produced via the (n,2n) reaction in most cases – at least 98%. A good agreement between the experimental and calculated reaction rates was achieved, as presented in **Table 2**. Generally, a measure of disagreement does not exceed more than slightly above one standard deviation. Moreover, the agreement is independent of the beam energy.
The results show that a combination of the simulated particle flux – especially the neutron spectra – and the employed cross sections describes the real conditions of the spallation experiment in a reliable way. This indicates that the ENDF/B-VII.0 data library and INCL4-ABLA physics models incorporated into MCNPX 2.7.0 perform well in the simulation of neutron production in the interval of energies where the ^{238}U(n,2n)^{237}U reaction plays an important role, i.e. from the energy threshold $E_{th} \cong 6.2$ MeV up to several tens MeV.

Table 2 Comparison of the experimental and calculated production of ^{237}U in natural uranium samples that is caused mainly via the ^{238}U(n,2n)^{237}U reaction. A contribution of deuterons and protons is lower than 2%.

Exp. Ident.	Beam Energy E_d (AGeV)	R_{exp}	R_{calc}	E/C
		10^{-26} (atom^{-1}·deuteron^{-1})		
M12	0.5	0.94(10)	0.82	**1.15(12)**
M12-Cd	0.5	0.91(9)	0.94	**0.97(10)**
M11	1	2.13(23)	2.60	**0.82(9)**
M11	2	3.9(4)	3.43	**1.14(14)**
M12	2	5.1(5)	4.47	**1.15(13)**
M12-Cd	2	3.5(3)	3.38	**1.03(11)**
M11	3	4.4(6)	4.97	**0.89(12)**
M12	4	8.9(11)	6.85	**1.30(16)**
M12-Cd	4	8.2(9)	7.23	**1.14(13)**

5.2. Production of ^{239}U

The production of ^{239}U from ^{238}U according to Eq. (2) – with the use of the MCNPX 2.7.0 code to calculate the particle flux and ENDF/B-VII.0 ($E_n \leq 20$ MeV), JENDL-HE/2007 ($E_n > 20$ MeV), and TALYS (proton-, deuteron-induced reactions) for determination of the cross sections – has shown that the ^{239}U isotope, including its daughter ^{239}Np, is produced via the (n,γ) reaction in more than 99 out of 100 cases. A comparison between the experimental and calculated reaction rates is presented in **Table 3**. An agreement within one, alternatively two standard deviations was achieved. The comparison does not reveal any obvious dependence on beam energy.

The comparison shows that the Monte Carlo simulation of particle flux – especially neutrons – and the used cross sections perform reliably in the description of conditions of the spallation experiment. The results revealed that the MCNPX 2.7.0 code employing the ENDF/B-VII.0 data library and INCL4-ABLA physics models describes properly the neutron production and transport in the region of energies with great importance to the ^{238}U(n,γ)^{239}U reaction, i.e. from thermal energies up to $E_n \cong$ 3 MeV.

In **Table 4**, there is presented a comparison of the experimental spectral indices SI_{exp} and calculated spectral indices SI_{calc} that describe a production of both ^{237}U and ^{239}U in ^{238}U. According to the results of simulation, the neutron-induced generation of these isotopes, i.e. the (n,2n)/(n,γ) spectral index, represents approx. 98% of the total production induced by neutrons, protons, and deuterons. The main advantage of the spectral indices consists in the reduction in the total experimental uncertainty of the uncertainty in determination of the beam integral. A general agreement between the experiment and simulation was reached without any obvious dependence on the beam energy.

Table 3 Comparison of the experimental and calculated production of ^{239}U. Experimental values are based on measurements of ^{239}Np. The main role in its production plays the ^{238}U(n,γ)^{239}U reaction. A contribution of deuteron- and proton-induced generation of ^{239}Np is below 1%.

Exp. Ident.	Beam Energy E_d (AGeV)	R_{exp}	R_{calc}	E/C
		10^{-26} (atom^{-1}·deuteron^{-1})		
M12	0.5	2.6(3)	2.28	**1.16(14)**
M12-Cd	0.5	2.55(29)	2.35	**1.08(12)**
M11	1	5.0(6)	4.70	**1.07(13)**
M11	2	8.5(9)	7.34	**1.16(13)**
M12	2	9.8(11)	8.11	**1.21(14)**
M12-Cd	2	9.4(10)	7.85	**1.20(13)**

M11	3	10(1)	9.75	**1.02(12)**
M12	4	16.8(19)	13.3	**1.26(14)**
M12-Cd	4	16.2(19)	13.4	**1.21(14)**

Table 4 Comparison of the experimental and calculated spectral indices for the production of ^{237}U and ^{239}U in ^{238}U. Simulation of neutron-, proton-, and deuteron-induced generation considered. A contribution of the (n,2n)/(n,γ) spectral index to the total production is approx. 98%.

Exp. Ident.	**Beam Energy** E_d (AGeV)	**(n,2n)/(n,γ) spectral index**		
		SI_{exp}	SI_{calc}	E/C
M12	0.5	0.36(2)	0.36	**0.99(7)**
M12-Cd	0.5	0.36(2)	0.40	**0.90(5)**
M11	1	0.42(2)	0.55	**0.77(4)**
M11	2	0.46(4)	0.47	**0.99(8)**
M12	2	0.53(3)	0.55	**0.96(6)**
M12-Cd	2	0.37(2)	0.43	**0.87(4)**
M11	3	0.44(4)	0.51	**0.87(9)**
M12	4	0.53(4)	0.51	**1.04(8)**
M12-Cd	4	0.51(3)	0.54	**0.95(6)**

5.3. Fission rate in ^{nat}U

The fission rate in natural uranium samples was calculated according to Eq. (2) – employing the MCNPX 2.7.0 code to calculate the particle flux and ENDF/B-VII.0 ($E_n \leq 20$ MeV) with JENDL-HE/2007 ($E_n > 20$ MeV) to obtain the reaction cross sections.

The experimental fission rate is based on the weighted mean of the fission rates of up to 27 carefully selected fission fragments divided by the cumulative fission yields taken from the ENDF/B-VII.1 library. To make a comparison between experiment and simulation, the fission yields Y_z^{nat} calculated according to Eq. (3) were used. A comparison employing the weighted fission yields $Y_{z,w}^{nat}$ (Eq. (4)-(6)) resembles the results obtained using the fission yields Y_z^{nat}. The experimental fission rates and the results of simulation are compared in **Table 5**.

The reaction rates based on the calculation of neutron-, proton-, and deuteron-induced fission are presented in the column R_{calc}^{NPD}. A corresponding comparison with experiment is introduced as a ratio E/C^{NPD}. One can see that the calculated fission rate R_{calc}^{NPD} is somewhat overestimated in comparison with the experimental data, in some cases beyond three standard deviations.

In **Table 5**, there are also presented the fission rates R_{calc}^{N} calculated according to the Eq. (2), but when taking into account the neutron-induced fission exclusively. A corresponding comparison with the experiment E/C^{N} revealed that the R_{calc}^{N} values fit the experimental data more appropriately than the R_{calc}^{NPD} fission rate.

A comparison of the experimental spectral indices to the calculated indices for the fission rate induced by neutrons, protons, and deuterons (SI_{calc}^{NPD}) and the total production of ^{239}U and its decay products – ^{239}Np and ^{239}Pu – is presented in **Table 6**. The E/C^{NPD} ratio shows that the calculated spectral indices are overestimated at all beam energies. Nevertheless, taking into account exclusively the neutron flux and the corresponding (n,f)/(n,γ) spectral index (SI_{calc}^{N}), the E/C^{N} ratio reveals a closer agreement between experiment and simulation within two standard deviations in most cases.

Table 5 Comparison of the experimental and calculated fission reaction rate in natural uranium samples. Calculation of the fission yields is based on the F.E. (see Eq. (3)) and S.C. (see Eq. (6)) methods. The neutron-, proton-, and deuteron-induced fission is considered in R_{calc}^{NPD} and the corresponding ratio E/C^{NPD} between experiment and calculation is based on the F.E.

experimental values. Exclusively the neutron spectra are taken into consideration in calculated reaction rate R^N_{calc}. The corresponding ratio E/C^N is based on the F.E. method as well.

Exp. Ident.	E_d (AGeV)	R_{exp} (F.E.)	R_{exp} (S.C.)	R^{NPD}_{calc}	R^N_{calc}	E/C^{NPD}	E/C^N
		10^{-25} (atom^{-1}·deuteron^{-1})					
M12	0.5	0.63(7)	0.60(6)	0.80	0.49	**0.78(9)**	**1.27(15)**
M12-Cd	0.5	0.53(6)	0.51(5)	1.11	0.58	**0.47(6)**	**0.91(11)**
M11	1	0.99(11)	0.97(11)	2.76	1.46	**0.36(4)**	**0.67(8)**
M11	2	1.76(20)	1.71(19)	1.99	1.65	**0.88(10)**	**1.06(12)**
M12	2	2.4(3)	2.35(27)	3.54	2.30	**0.69(8)**	**1.06(13)**
M12-Cd	2	1.68(20)	1.65(18)	1.88	1.62	**0.9(1)**	**1.04(12)**
M11	3	1.99(22)	1.99(22)	3.28	2.46	**0.61(7)**	**0.81(9)**
M12	4	4.0(4)	3.8(4)	4.42	3.37	**0.9(1)**	**1.18(13)**
M12-Cd	4	3.7(4)	3.6(4)	5.07	3.62	**0.73(9)**	**1.02(13)**

Table 6 Comparison between the experimental spectral indices SI_{exp} and the results of simulation SI_{calc} of the fission rate in the natural uranium samples and production of ^{239}U from ^{238}U. Simulation of neutron-, proton-, and deuteron-induced fission (see Eq. (2)) is considered in SI^{NPD}_{calc} as well as in the corresponding comparison E/C^{NPD}. Exclusively the neutron-induced fission is taken into account in SI^N_{calc} and in the ratio E/C^N.

Exp. Ident.	E_d (AGeV)	Fission / ^{239}U production			(n,f)/(n,γ) spectral index	
		SI_{exp}	SI^{NPD}_{calc}	E/C^{NPD}	SI^N_{calc}	E/C^N
M12	0.5	2.36(20)	3.53	**0.67(6)**	2.16	**1.10(9)**
M12-Cd	0.5	2.06(15)	4.71	**0.44(3)**	2.47	**0.84(6)**
M11	1	1.96(15)	5.86	**0.33(3)**	3.11	**0.63(5)**
M11	2	2.07(13)	2.71	**0.76(5)**	2.25	**0.92(6)**
M12	2	2.49(20)	4.36	**0.57(5)**	2.83	**0.88(7)**
M12-Cd	2	1.79(11)	2.39	**0.75(5)**	2.07	**0.87(6)**
M11	3	1.99(13)	3.36	**0.59(4)**	2.53	**0.79(5)**
M12	4	2.38(15)	3.32	**0.72(5)**	2.53	**0.94(6)**
M12-Cd	4	2.28(19)	3.77	**0.61(5)**	2.69	**0.85(7)**

5.4. Discussion

The results on ^{238}U(n,2n)^{237}U and ^{238}U(n,γ)^{239}U reactions have shown that there is a general agreement between the experimental reaction rates and results of simulation of particle flux using the MCNPX 2.7.0 code (see **Table 2**, **Table 3**, **Table 4**). The experimental fission rate is also in agreement – mostly within two standard deviations – with the calculated fission rate in the case that the proton- and deuteron-induced fission is omitted. A comparison of the spectral indices brings the similar results (see **Table 5**, **Table 6**).

The following conclusion can be drawn: the MCNPX 2.7.0 code employing the ENDF/B-VII.0 data library and INCL4-ABLA physics models performs well in both the neutron production and transport in the region of energies with crucial importance to the ^{238}U(n,2n)^{237}U and ^{238}U(n,γ)^{239}U reactions, i.e. from thermal energies up to several tens MeV.

Moreover, the results show that the Monte Carlo simulation describes the neutron-induced fission in a reliable way as well. It is worth mentioning that according to the results of simulation, more than 98% of the neutron-induced fissions in the uranium samples is initiated by neutrons with energy $E_n > 1$ MeV (see also **Fig. 1c**). Thus a worsened agreement in some cases – i.e. the E/C^N ratio beyond one standard deviation in **Table 5** – is not caused by the spectrum-dependent effects in the resonance

region but emerges on account of effects above this value. Obviously, some discrepancy may come from the data in the JENDL-HE/2007 library used for calculation of the fission cross section above 20 MeV in Eq. (2) (on average, 44% of the neutron-induced fissions in the samples was initiated by neutrons with energy $E_n > 20$ MeV).
The authors suppose that the disagreement in the total calculated fission rate induced by neutrons, protons, and deuterons R_{calc}^{NPD} (see **Table 5**), as well as regarding the corresponding spectral indices SI_{calc}^{NPD} (see **Table 6**) stems either from the overestimation in proton or deuteron production in Monte Carlo simulation or from the overvaluation of the cross section for fission initiated by protons in the JENDL-HE/2007 library and the inappropriately derived deuteron-induced-fission cross section used to calculate the reaction rate according to Eq. (2). To prove the latter, more experimental data on interactions of protons and deuterons with uranium at higher energies are needed.

6. Conclusion

A comparison between the experimental reaction rates in the natural uranium samples irradiated in the central region of the uranium spallation target *QUINTA* and the reaction rates calculated using the Monte Carlo simulation of particle flux and corresponding cross-section data was presented in this article. The uranium samples were activated in the combined field of spallation neutrons, fission neutrons, neutrons generated in the (n,*x*n) reactions, and scattered neutrons in the place where the maximum neutron flux was expected. Nevertheless, in this position, a contribution of charged particles – primary deuterons of energy from 0.5 AGeV up to 4 AGeV and protons released in the deuteron break-up and intranuclear cascade – to the total reaction rate must be taken into consideration.
In fact, the impact of deuterons and protons on the production of ^{237}U and ^{239}U is rather insignificant since the reaction cross sections at GeV energies are low in comparison with the cross sections for the ^{238}U(n,2n)^{237}U and ^{238}U(n,γ)^{239}U reactions in the whole interval of energies of produced neutrons. On the other hand, a contribution of the deuteron- and proton-induced fission to the total fission rate in the natural uranium samples cannot be omitted.
A comparison between the experimental and simulated reaction rates of the radiative capture and the (n,2n) reaction in ^{238}U (**Table 2**, **Table 3**) as well as the (n,2n)/(n,γ) spectral indices (**Table 4**) revealed a general agreement, generally within or slightly beyond one standard deviation, which points out to the fact that the generation, transport, and interactions of neutrons with energy up to several tens MeV are well performed in the MCNPX 2.7.0 code using the ENDF/B-VII.0 nuclear data library and the INCL4-ABLA physics models. The simulated neutron flux was combined with the reaction cross section adopted from the ENDF/B-VII.0 and JENDL-HE/2007 libraries and TALYS-1.6 code.
The authors assume that the comparison E/C^{NPD} between the experimental and calculated fission rates indicates that the calculation of deuteron- and proton-induced fission is overestimated (**Table 5**). The overvaluation can come either from the increased charged-particle flux or from the corresponding cross sections based on the JENDL-HE/2007 library. A reasonably good agreement was reached when the experimental fission rate was compared to the calculated rate of fission induced exclusively by neutrons of all energies. A comparison of the (n,f)/(n,γ) spectral index revealed similar behaviour (**Table 6**).
This assumption is supported by the results of the recent study [51] on transmutation of the transuranium samples (^{237}Np, ^{238}Pu, ^{239}Pu) in the peripheral region of the *QUINTA* target assembly where the contribution of primary deuterons and secondary protons is negligible. In this case, a good agreement within one standard deviation was reached in most cases of comparison between the experiment and calculation of fission transmutation rates using the MCNPX 2.7.0 code and ENDF/B-VII.0 and JENDL-HE/2007 neutron data libraries.
As the results show, both the experimental and calculated reaction rates increase proportionally to the deuteron beam energy generally within one or two standard deviations, which was additionally confirmed by the independent calculations of the fission rate using the MCNPX code 2.7.e with the

ISABEL-ABLA-LAQGSM [52],[53] physics models as well as the MARS15 code [54],[55] employing the LAQGSM03.03 [56] event generator.

Acknowledgements

The authors are grateful for the financial support allocated by the Grants "3+3" and the Grants of the Plenipotentiary of the Government of the Czech Republic in JINR that helped to conduct this research in the period between 2011 and 2013.

References

[1] F. Carminati, et al., CERN/AT/93-47 (ET), Geneva, (1993).
[2] C.D. Bowman, et al. Nuclear Instruments and Methods in Physics Research A **320** (1992) 336.
[3] S. Andriamonje, et al., Physics Letters B **348** (1995) 697.
[4] D. Hilscher, et al., Nuclear Instruments and Methods in Physics Research A **414** (1998) 100.
[5] A. Letourneau, et al. Nuclear Instruments and Methods in Physics Research B **170** (2000) 299.
[6] A. Abánades, et al., Nuclear Instruments and Methods in Physics Research A **463** (2001) 586.
[7] A. Krása, et al., Nuclear Instruments and Methods in Physics Research A **615** (2010) 70.
[8] D. Heuer, et al., Annals of Nuclear Energy **64** (2014) 421.
[9] J. Serp, et al, Progress in Nuclear Energy **77** (2014) 308.
[10] J. Adam, et al., JINR Preprint E1-2010-61, Dubna, 2010.
[11] V.I. Yurevich, et al., Physics of Particles and Nuclei Letters **3** (2006) 169.
[12] V.I. Yurevich, Physics of Particles and Nuclei **41** (2010) 778.
[13] J. Taieb, et al., Proc. of Int. Conf. on Nuclear Data for Science and Technology 2007, Apr 22 – 27, Nice, France, 1 (2008) 429.
[14] M. Soleilhac, et al, Journal of Nuclear Energy **23** (1969) 257.
[15] T. Ethvignot, et al., Physical Review Letters **94** (2005) 052701.
[16] I. Asplund-Nilsson, et al., Nuclear Science and Engineering **20** (1964) 527.
[17] J.-S. Wan, et al., Nuclear Instruments and Methods in Physics Research A **463** (2001) 634.
[18] J. Adam, et al., European Physical Journal A **47** (2011) 85.
[19] S.R. Hashemi-Nezhad, et al., Nuclear Instruments and Methods in Physics Research A **591** (2008) 517.
[20] http://e-t.jinr.ru.
[21] J.J. Borger, et al., Nuclear Instruments and Methods in Physics Research A **664** (2012) 103.
[22] W. Furman, et al., Proc. of Int. Baldin Seminar on High Energy Physics Problems, Dubna, Sep 10 – 15, PoS(Baldinn ISHEPP XXI)086, 2012.
[23] N.L. Asquith, et al., Annals of Nuclear Energy **63** (2014) 742.
[24] J.Adam, et al, JINR Preprint P1-2012-147, Dubna, 2013.
[25] I.V. Zhuk, et al., Radiation Measurements **43** (2008) S210.
[26] J. Frána, Journal of Radioanalytical and Nuclear Chemistry **257** (2003) 583.
[27] Evaluated Nuclear Structure Data File (ENSDF) Retrieval <http://www.nndc.bnl.gov/ensdf/>.
[28] L.P. Ekstrom, R.B. Firestone, WWW Table of Radioactive Isotopes, database version 2/28/99 < http://ie.lbl.gov/toi/index.htm >.
[29] K. Debertin and R.G. Helmer, Gamma- and X-ray Spectrometry with Semiconductor Detectors, Elsevier Science Publishers B.V., Amsterdam, The Netherlands, 1988.
[30] M. Suchopár, et al., Proc. of Int. Baldin Seminar on High Energy Physics Problems, Dubna, Sep 10 – 15, PoS (Baldin ISHEP XXI)091, 2012.
[31] D.B. Pelowitz, MCNPX Version 2.7.0, LA-CP-11-00438, 2011.
[32] M.B. Chadwick, et al., Nuclear Data Sheets **107** (2006) 2931.
[33] A. Boudard, et al., Physical Review C **66** (2002) 044615.

[34] A.R. Junghans, et al., Nuclear Physics A **629** (1998) 635.
[35] JENDL High Energy File 2007, < http://wwwndc.jaea.go.jp/ftpnd/jendl/jendl-he-2007.html>.
[36] A. Koning, et al., TALYS-1.6, A nuclear reaction program, NRG Petten, The Netherlands, 2013.
[37] A.J. Koning, et al., Nuclear Data Sheets **118** (2014) 187.
[38] NJOY 99.0, PSR-480, ORNL, TN-USA, 1999. V 99.393 <http://t2.lanl.gov/nis/codes.shtml>.
[39] O.E. Shigaev, et al., Khlopin Radiev. Inst., Leningrad Reports **17** (1973).
[40] V.S. Bychenkov, et al., Yadernaya Fizika **17** (1973) 947.
[41] V.A. Konshin, et al., Yadernaya Fizika **2** (1965) 682.
[42] P.C. Stevenson, et al., Physical Review **111** (1958) 886.
[43] N.S. Ivanova, Zhurnal Exp. i Teoret. Fiziki **31** (1956) 413.
[44] A.A. Kotov, et al., Physical Review C **74** (2006) 034605.
[45] V.I. Yurevich, et al., Yadernaya Fizika **65** (2002) 1417.
[46] B.A. Bochagov, et al., Yadernaya Fizika **28** (1978) 572.
[47] L.N. Andronenko, et al., Yadernaya Fizika **24** (1976) 671.
[48] S. Stoulos, et al., Physical Review C **85** (2012) 024612.
[49] A.J. Koning, D. Rochman, Nuclear Data Sheets **113** (2012) 2841.
[50] M.B. Chadwick, et al., Nuclear Data Sheets **112** (2011) 2887.
[51] L. Zavorka, et al., Neutron-induced transmutation reactions in ^{237}Np, ^{238}Pu, and ^{239}Pu at the massive natural uranium spallation target, accepted for the publication in Nuclear Instruments and Methods in Physics Research B.
[52] Y. Yariv, Z. Fraenkel, Physical Review C **24** (1981) 488.
[53] S.G. Mashnik, et al., LANL Report LA-UR-08-2931, 2008.
[54] N.V. Mokhov, et al., Technical Report FERMILAB-CONF-12-635-APC, 2012.
[55] N.V. Mokhov, et al., AIP Conference Proceedings **896** (2007) 50.
[56] N. Mokhov, et al., Progress in Nuclear Science and Technology **4** (2014) 496.

Appendix

Table 7 Experimental reaction rates for fission in ^{nat}U divided by the corresponding fission yield. The results of the F.E. (calculation of yields according to Eq. (3)) and S.C. (yields based on Eq. (6)) methods are presented. Systematic uncertainty in beam monitoring is not included.

Exp. Ident.	**M12**				**M12-Cd**				**M11**			
Beam Energy (AGeV)	**0.5**				**0.5**				**1**			
Method	**F.E.**		**S.C.**		**F.E.**		**S.C.**		**F.E.**		**S.C.**	
Fission product	**Reaction rate/Cumulative fission yield R_{exp}^{CY} 10^{-25} (atom^{-1}·deuteron^{-1})**											
	R_{exp}^{CY}	ΔR_{exp}^{CY}	R_{exp}^{CY}	ΔR_{exp}^{CY}	R_{exp}^{CY}	ΔR_{exp}^{CY}	R_{exp}^{CY}	ΔR_{exp}^{CY}	R_{exp}^{CY}	ΔR_{exp}^{CY}	R_{exp}^{CY}	ΔR_{exp}^{CY}
^{85m}Kr	0.82	0.09	0.92	0.07	0.72	0.03	0.80	0.02	1.31	0.10	1.44	0.08
^{87}Kr	0.66	0.06	0.67	0.05	0.63	0.05	0.64	0.03	0.99	0.08	1.0	0.06
^{88}Kr					0.57	0.04	0.59	0.03	1.02	0.11	1.04	0.08
^{91}Sr	0.66	0.02	0.65	0.02	0.57	0.04	0.56	0.03	1.03	0.08	1.01	0.05
^{92}Sr	0.59	0.03	0.56	0.02	0.54	0.04	0.52	0.03	1.03	0.09	0.99	0.06
^{93}Y	0.59	0.05	0.56	0.03	0.55	0.04	0.53	0.03	1.02	0.15	0.99	0.11
^{95}Zr	1.85	0.07	1.81	0.05	0.90	0.20	0.88	0.14	1.08	0.04	1.07	0.03
^{97}Zr	0.68	0.02	0.67	0.01	0.62	0.03	0.61	0.02	1.10	0.04	1.08	0.03
^{99}Mo	0.71	0.04	0.69	0.03	0.67	0.06	0.65	0.04	1.22	0.08	1.19	0.05

^{103}Ru	1.61	0.06	1.40	0.04	0.91	0.04	0.80	0.02	1.32	0.04	1.18	0.02
^{105}Ru	0.97	0.04	0.87	0.02	0.82	0.03	0.74	0.02	1.39	0.05	1.26	0.03
^{107}Rh	1.66	0.31	1.65	0.22	1.22	0.21	1.26	0.16				
^{113}Ag	3.67	0.35	4.18	0.28	2.32	0.18	3.06	0.17				
^{115}Cd	2.29	0.10	2.57	0.08	1.70	0.11	2.29	0.10	3.25	0.18	3.26	0.12
^{117m}Cd												
^{117}Cd	1.39	0.17	1.70	0.15	0.96	0.07	1.36	0.07				
^{125}Sn												
^{127}Sb	0.54	0.05	0.82	0.05	0.48	0.02	0.72	0.03	0.79	0.05	1.07	0.05
^{129}Sb												
^{131}I	0.47	0.02	0.51	0.01	0.39	0.02	0.42	0.01	0.83	0.02	0.88	0.02
^{133}I	0.49	0.04	0.47	0.03	0.48	0.05	0.46	0.03	0.91	0.07	0.87	0.04
^{134}Te	0.55	0.13	0.47	0.08	0.43	0.04	0.38	0.02				
^{135}I	0.45	0.02	0.41	0.01	0.43	0.01	0.39	0.01	0.82	0.03	0.76	0.02
^{140}Ba	0.66	0.04	0.59	0.02	0.59	0.09	0.54	0.06	1.05	0.04	0.96	0.02
^{143}Ce	0.50	0.03	0.47	0.02	0.47	0.02	0.44	0.01	0.91	0.03	0.86	0.02
^{147}Nd									1.06	0.11	0.98	0.07
^{149}Nd	0.62	0.08	0.60	0.05	0.52	0.05	0.50	0.04				

Table 7 (Continued.)

Exp. Ident.	**M11**				**M12**				**M12-Cd**			
Beam Energy (AGeV)	**2**				**2**				**2**			
Method	**F.E.**		**S.C.**		**F.E.**		**S.C.**		**F.E.**		**S.C.**	
Fission product	**Reaction rate/Cumulative fission yield R_{exp}^{CY} 10^{-25} (atom^{-1}·deuteron^{-1})**											
	R_{exp}^{CY}	ΔR_{exp}^{CY}	R_{exp}^{CY}	ΔR_{exp}^{CY}	R_{exp}^{CY}	ΔR_{exp}^{CY}	R_{exp}^{CY}	ΔR_{exp}^{CY}	R_{exp}^{CY}	ΔR_{exp}^{CY}	R_{exp}^{CY}	ΔR_{exp}^{CY}
^{85m}Kr	2.41	0.14	2.70	0.11	3.28	0.26	3.60	0.20	2.11	0.15	2.37	0.12
^{87}Kr	1.94	0.18	1.97	0.13	2.84	0.22	2.87	0.15	2.02	0.12	2.05	0.09
^{88}Kr	1.93	0.08	1.97	0.06					1.88	0.12	1.93	0.09
^{91}Sr	1.81	0.12	1.78	0.08	2.79	0.16	2.75	0.11	1.76	0.13	1.73	0.09
^{92}Sr	1.92	0.21	1.83	0.14	2.47	0.29	2.38	0.20	1.92	0.24	1.83	0.16
^{93}Y	2.33	0.29	2.24	0.21	3.41	0.21	3.28	0.16	1.97	0.15	1.90	0.10
^{95}Zr	2.02	0.06	1.98	0.04	2.45	0.15	2.41	0.11	1.70	0.09	1.66	0.06
^{97}Zr	1.91	0.10	1.87	0.07	2.61	0.18	2.56	0.13	1.93	0.29	1.88	0.20
^{99}Mo	1.99	0.26	1.93	0.18	3.24	0.56	3.15	0.39	2.19	0.30	2.11	0.21
^{103}Ru	2.18	0.06	1.89	0.04	3.53	0.14	3.13	0.09	2.20	0.08	1.91	0.05
^{105}Ru	2.39	0.08	2.13	0.05	4.01	0.29	3.63	0.19	2.28	0.10	2.04	0.06
^{107}Rh					6.55	0.94	6.45	0.66	3.68	0.57	3.82	0.42
^{113}Ag					11.6	1.4	12.3	1.1	4.31	0.34	6.10	0.34
^{115}Cd	5.06	0.20	5.70	0.16	9.01	0.40	9.21	0.29	3.73	0.22	5.39	0.22
^{117m}Cd					17.0	1.3	19.4	1.1	6.31	0.44	9.55	0.47
^{117}Cd					6.64	2.14	7.40	1.69	2.88	0.55	4.33	0.58
^{125}Sn					2.70	0.63	3.20	0.52	1.41	0.30	2.18	0.33
^{127}Sb	1.41	0.13	2.14	0.14	2.26	0.22	3.13	0.22	1.25	0.08	2.00	0.09
^{129}Sb	0.99	0.09	1.23	0.08	1.59	0.23	1.90	0.19	0.95	0.07	1.21	0.06
^{131}I	1.38	0.04	1.49	0.03	2.03	0.10	2.17	0.08	1.33	0.10	1.44	0.07

^{133}I	1.69	0.18	1.61	0.12	2.10	0.19	2.02	0.13	1.65	0.12	1.57	0.08
^{134}Te									1.91	0.27	1.63	0.16
^{135}I	1.58	0.04	1.43	0.03	1.99	0.08	1.83	0.05	1.57	0.03	1.41	0.02
^{140}Ba	1.79	0.06	1.61	0.04	2.35	0.14	2.15	0.09	2.02	0.13	1.81	0.08
^{143}Ce	1.72	0.08	1.60	0.05	1.91	0.10	1.79	0.07	1.63	0.19	1.51	0.12
^{147}Nd	1.60	0.13	1.45	0.08	1.94	0.25	1.79	0.16	1.53	0.19	1.39	0.12
^{149}Nd	1.98	0.19	1.89	0.13	3.55	0.69	3.41	0.47	1.90	0.14	1.81	0.10

Table 7 (Continued.)

Exp. Ident.	**M11**				**M12**				**M12-Cd**			
Beam Energy (AGeV)	**3**				**4**				**4**			
Method	**F.E.**		**S.C.**		**F.E.**		**S.C.**		**F.E.**		**S.C.**	
Fission product	**Reaction rate/Cumulative fission yield R_{exp}^{CY} 10^{-25} (atom^{-1}·deuteron^{-1})**											
	R_{exp}^{CY}	ΔR_{exp}^{CY}	R_{exp}^{CY}	ΔR_{exp}^{CY}	R_{exp}^{CY}	ΔR_{exp}^{CY}	R_{exp}^{CY}	ΔR_{exp}^{CY}	R_{exp}^{CY}	ΔR_{exp}^{CY}	R_{exp}^{CY}	ΔR_{exp}^{CY}
^{85m}Kr	2.62	0.15	2.90	0.11	5.19	1.04	5.74	0.82	5.10	0.54	5.61	0.42
^{87}Kr	2.43	0.15	2.46	0.11	4.48	0.49	4.53	0.35	4.34	0.50	4.39	0.36
^{88}Kr	2.36	0.11	2.41	0.08	4.40	0.39	4.50	0.28				
^{91}Sr	2.07	0.15	2.03	0.10	4.43	0.41	4.36	0.28	4.09	0.45	4.03	0.31
^{92}Sr	2.29	0.26	2.20	0.17	4.08	0.89	3.91	0.60	3.77	0.19	3.62	0.13
^{93}Y					4.55	0.33	4.37	0.24	4.43	0.34	4.30	0.22
^{95}Zr	2.14	0.28	2.10	0.19	4.80	0.22	4.71	0.15	4.29	0.27	4.22	0.19
^{97}Zr	2.17	0.04	2.12	0.03	4.47	0.12	4.38	0.09	4.39	0.37	4.31	0.25
^{99}Mo	2.35	0.21	2.28	0.14	4.01	0.35	3.90	0.24	4.04	0.54	3.92	0.37
^{103}Ru	2.44	0.06	2.14	0.04	5.84	0.24	5.14	0.15	5.14	0.38	4.55	0.24
^{105}Ru	2.85	0.13	2.56	0.08	5.77	0.24	5.20	0.15	5.43	0.30	4.93	0.19
^{107}Rh												
^{113}Ag					17.7	2.3	19.0	1.7	13.2	2.1	16.9	1.9
^{115}Cd	5.70	0.23	6.11	0.18	13.0	1.2	13.8	0.9	9.7	0.8	12.6	0.7
^{117m}Cd												
^{117}Cd					9.30	2.88	10.8	2.4	6.25	1.46	8.50	1.41
^{125}Sn												
^{127}Sb	1.56	0.10	2.27	0.10	3.90	0.28	5.61	0.28	3.45	0.36	5.0	0.4
^{129}Sb	1.22	0.09	1.49	0.08	2.32	0.65	2.82	0.56				
^{131}I	1.62	0.04	1.73	0.03	3.31	0.11	3.54	0.09	3.10	0.11	3.30	0.09
^{133}I	1.96	0.18	1.87	0.12	3.72	0.35	3.55	0.24	3.51	0.28	3.36	0.19
^{134}Te												
^{135}I	1.85	0.06	1.68	0.04	3.47	0.09	3.16	0.06	3.34	0.13	3.06	0.09
^{140}Ba	1.85	0.10	1.68	0.07	4.37	0.46	3.98	0.30	3.70	0.38	3.39	0.25
^{143}Ce	1.93	0.13	1.80	0.08	3.60	0.15	3.37	0.10	3.51	0.29	3.30	0.20
^{147}Nd	2.04	0.15	1.87	0.10	3.84	0.64	3.53	0.42				
^{149}Nd	2.56	0.19	2.45	0.13	6.31	6.18	6.05	4.19	5.50	3.75	5.28	2.55

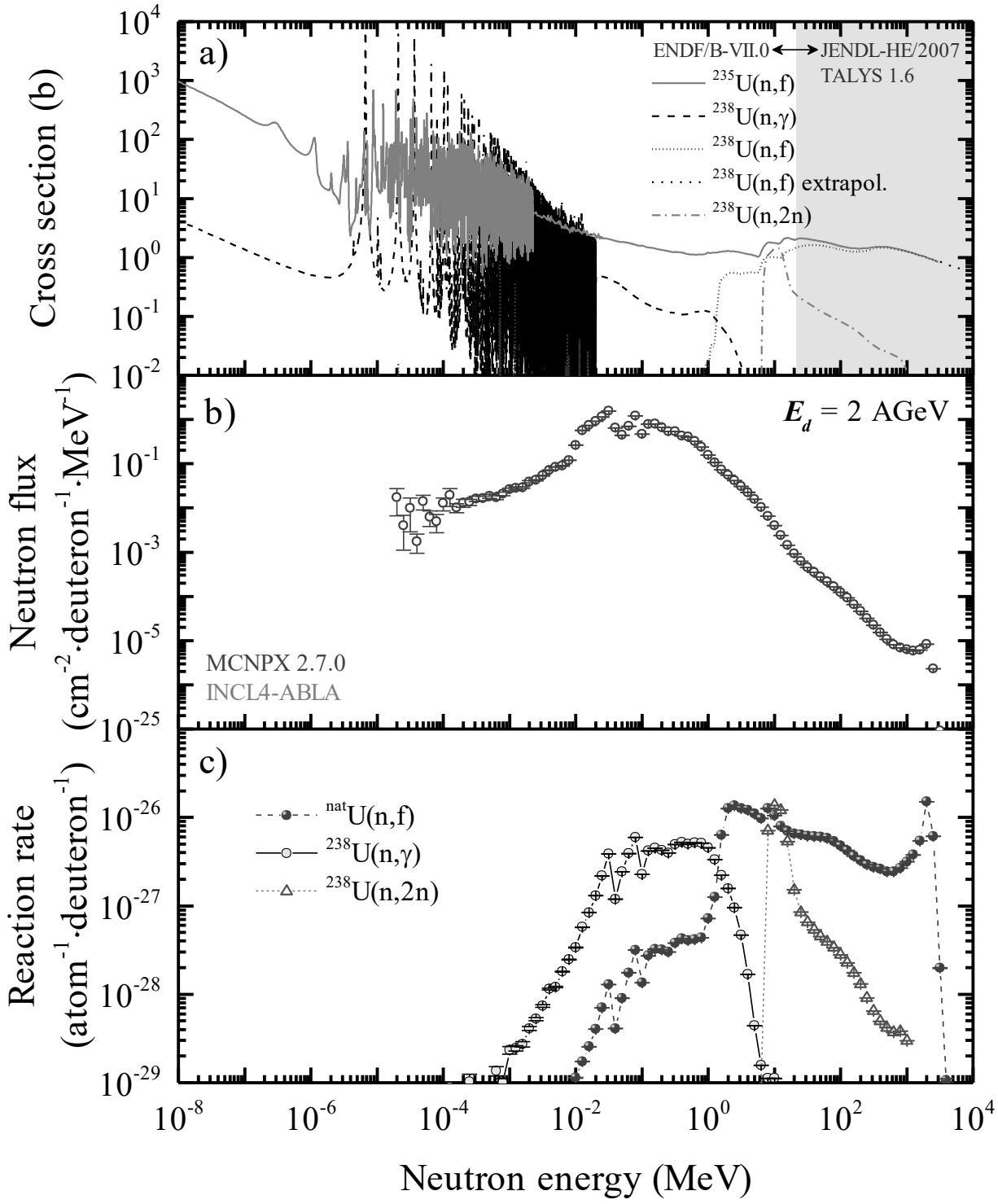

Fig. 1 **a)** Cross sections for the ^{238}U(n,γ)^{239}U and ^{238}U(n,2n)^{237}U reactions and neutron-induced fission in both ^{235}U and ^{238}U; **b)** Result of the MCNPX simulation of the neutron flux in ^{nat}U sample during the 2-AGeV irradiation; **c)** Calculated reaction rates, i.e. a convolution of the neutron

flux and the cross sections for the (n,γ) and (n,2n) reaction in ^{238}U and (n,f) in ^{nat}U. The energy intervals where the reactions play a dominant role can be clearly seen.

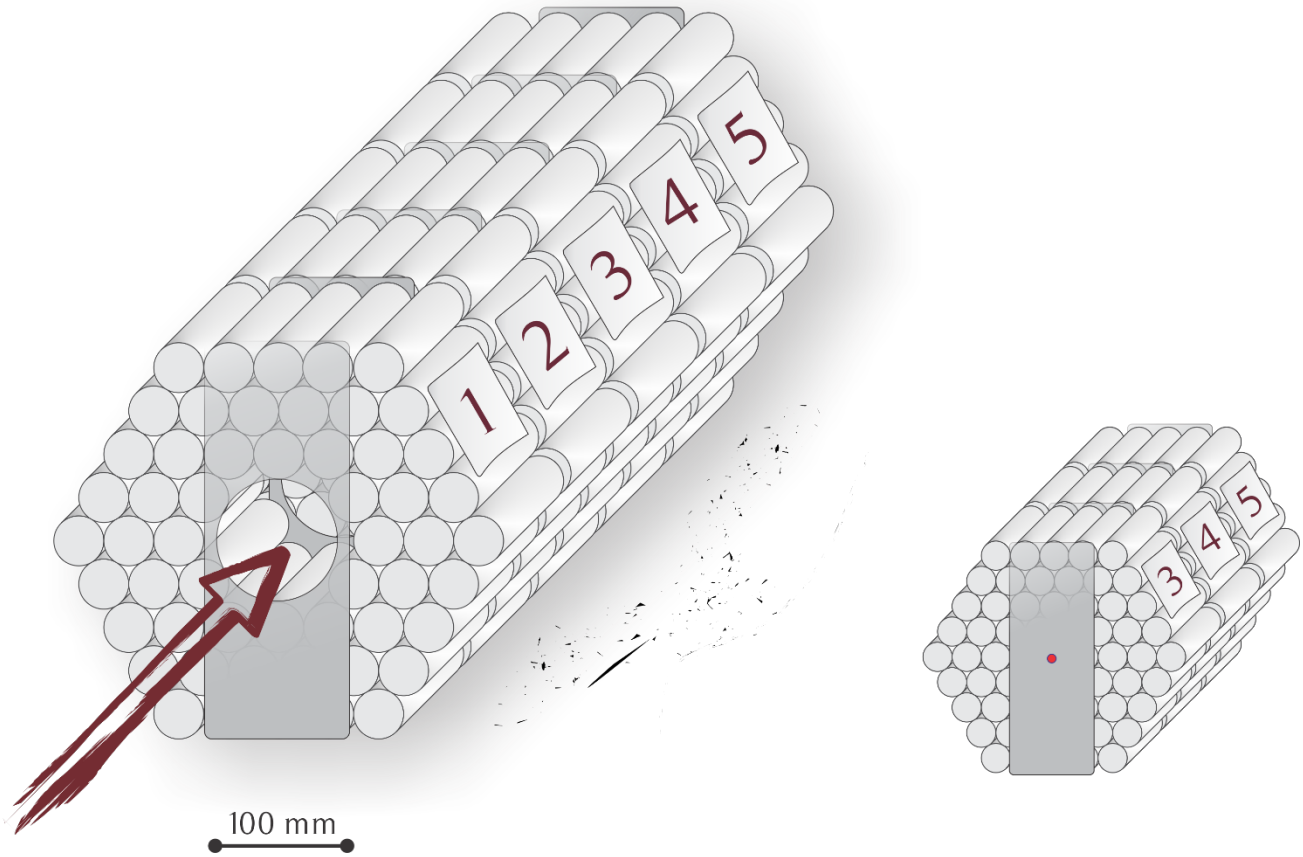

Fig. 2 Schematic drawing of the *QUINTA* target. An illustration of the deuteron beam impinging on the spallation target (left). Location of the natural uranium samples between the second and the third section of the target (right). Aluminium casing and lead shielding not displayed.

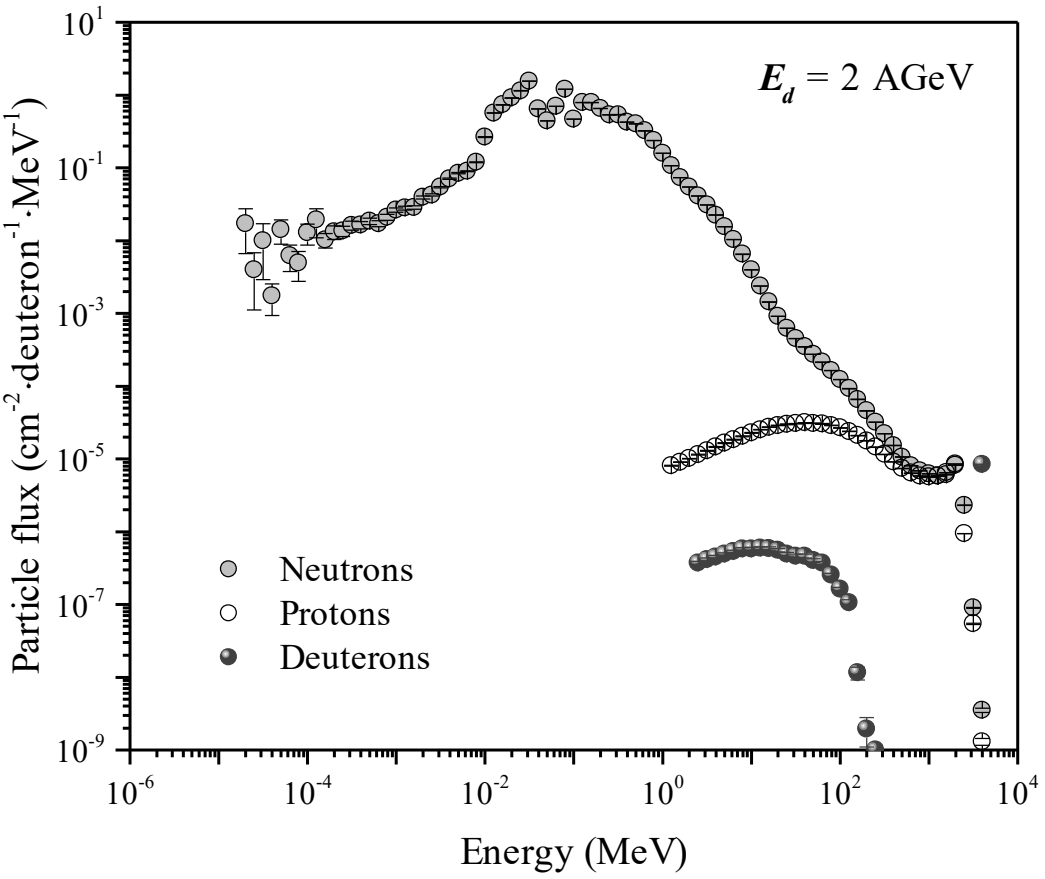

Fig. 3 Monte Carlo simulation of neutron, proton, and deuteron flux at the position of the natural uranium sample inside the *QUINTA* target during the irradiation with 2-AGeV deuterons.

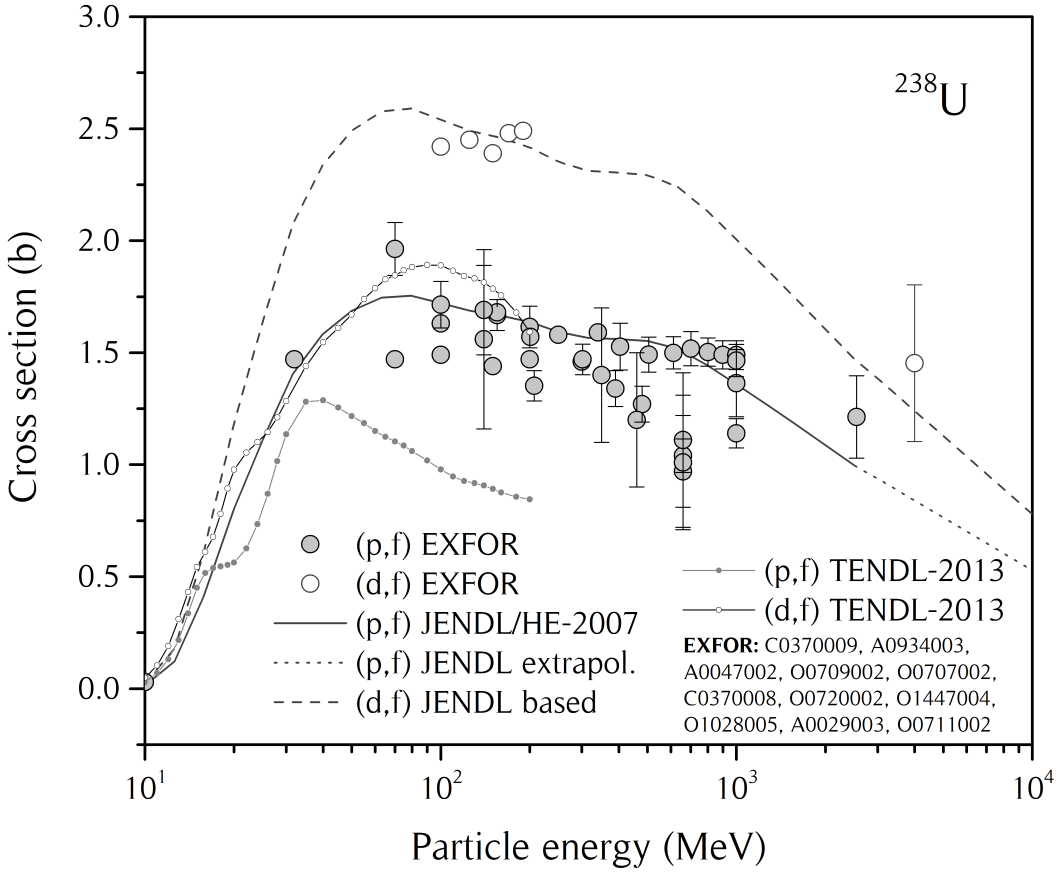

Fig. 4 Determination of the ^{238}U(d,f) reaction cross section based on the experimental data on (d,f) and evaluated data on (p,f) reaction in ^{238}U taken from the JENDL/HE-2007 library. For comparison, the TENDL-2013 evaluated data and the experimental data on (p,f) are displayed. Above 3 GeV, the cross sections were extrapolated.